A Self-Mixing Laser Sensor Design With an Extended Kalman Filter for Optimal Online Structural Analysis and Damping Evaluation

Caroline Bés, Victorien Belloeil, *Fellow, IEEE*, Guy Plantier, *Member, IEEE*, Yves Gourinat, and Thierry Bosch, *Senior Member, IEEE*

Abstract—We have developed a new algorithm based on the extended Kalman filter in order to improve the resolution of a self-mixing (SM) optical displacement sensor. This noncontact sensor, which provides vibration measurement with a very high accuracy, can be used for online quality control, for example, measuring the damping of excited mechanical structures. This SM sensor subject to weak feedback has been tested in comparison with a commercial vibrometer in order to measure the frequency response function (FRF) of a plate with a passive damping to be characterized, and to show the efficiency of a damping treatment.

Index Terms—Displacement sensors, extended Kalman filter, optical interferometry, structural analysis, vibration measurement.

I. INTRODUCTION

STRUCTURAL vibrations are undesirable as they can create disturbances like structural fatigue, transmission of vibrations to another system, or generate noise due to the acoustical radiation. However, vibrations and noise in a dynamic system can be reduced by a number of means. Firstly, to reduce noise, a negative noise from another source can be used. A second method consists in isolating the vibration to avoid any transmission to another system.

The third technique, known as passive damping, enables us to decrease the amplitude of vibrations. It has been the dominant technology in the noncommercial aerospace industry since the early 1960s [1], but the use of surface damping in the automotive, commercial airplane, appliance, and other industries has only been effective in recent years. In the aerospace sector, for example, it might be useful to test the efficiency of surface damping treatments on mechanical structures submitted to vibration online. This requires a modal analysis: 1) several points of the structure have to be tested at the same time, so several sensors must be used for a one-shot acquisition or 2) the sensor have to be placed at different locations and the measurement repeated, which is time consuming. Commercial vibrometers are excluded because they are too expensive to be duplicated for a sensor network. Traditional accelerometers cannot be used because contact measurements on a thin material modify the eigenmodes and the resonance frequencies. Noncontact measurements are required. Vibrometers with multiple probes using gaz lasers have also been proposed to measure out-of-plane surface velocities at different points of a structure surface [2]–[4]. But these setups are bulky due to the size of gaz laser configurations and the optical components required.

In this paper, we describe a new low-cost optical sensor. It has been tested to measure the frequency response function (FRF) of a plate with passive damping [5] submitted to a sweep sine excitation.

Generally, noncontact measurement of displacement and vibration using a laser is a very efficient method. However, such laser-based sensing systems require high-precision alignment and optical components such as mirrors and beam splitters. On the other hand, a displacement sensor based on the self-mixing (SM) principle does not need these expensive components. In such a sensor, a low-cost laser diode (LD) in its package (including a photodiode) highlights the vibrating target, and a part of the laser beam is then reinjected into the active cavity of the laser, where it interferes with the standing wave [6]. Such an interference generates a modulation of the optical output power (OOP) [7]. This modulation is then monitored by the photodiode included in the package of the LD, each fringe period being related to an optical path difference of half a wavelength ($\lambda/2$). The fringes are not a cosine function as in conventional interferometry but saw-tooth like, as interference occurs in the active cavity with an imaginary refractive index. Such a sensor is very user friendly; it is self-aligned as the emitted and the backscattered laser beam follow the same optical path, and the entire detection system is carried out in the compact package of the LD.

SM interference is a well-known effect studied extensively during the last four decades. Presently, sensors based on this physical phenomenon have been designed for a large number of applications. Absolute distance [8], displacement [9], velocity and vibration measurements [10], [11], modal analysis [12], as well as velocity measurement of fluids [13], have notably been demonstrated since the 80's [14], [15]. Early signal-processing simply involved performing a derivative of the SM signal and counting the occurrence of the negative and positive pulses obtained. By this means, the target displacement can be retrieved

with a $\lambda/2$ resolution. Later, different techniques were proposed in order to increase the resolution.

- A signal processing scheme based on the linearization of the fringe of the saw-tooth-like optical power was proposed. A resolution of $\lambda/12$, i.e., 70 nm with $\lambda = 785$ nm, was obtained [16].
- A fast modulation of the laser diode current causing a wavelength shift, which produces a phase dithering, was proposed. The resolution increased by sampling the SM signal synchronously with the dither [17].
- The SM signal was sampled and processed with a function inversion in order to extract the displacement included in the expression of the optical signal [18].

These two last methods provide a resolution of 40 nm, but require carefully controlled experimental conditions.

To our knowledge, "evolved" signal processing using adaptive algorithm applied to SM has never been reported, except for the SM LD velocimetry, where a second-order autoregressive (AR) estimation of the velocity [19] and maximum likelihood doppler-frequency estimation [10] have been proposed. The other example is the design of an SM displacement sensor based on the unwrapping of the phase estimation [see (1)–(3)] [20] and a wavelet transform when the signal is noisy due to hostile industrial environnement [21]. Unfortunately, this method is dedicated to moderate feedback at present.

For our application, we consider only the weak feedback regime, i.e., the SM phenomenon when only a part of the light reenters the active cavity. The signal is then slightly nonlinear, but still allows a linearized model to be determined, hence, enabling us to use the suboptimal extended Kalman filter.

The paper is organized as follows. Section II presents the model behavior of the SM signal for $C < 1$ and its use with an extended Kalman filter to extract the displacement from the OOP. Our algorithm is tested in Section III. The application of our sensor for online damping measurements is explained in Section IV.

II. DISPLACEMENT RECONSTRUCTION ALGORITHM

A. Basic SM Principle

The theory of SM interferometry is now well known [22]. A complete analysis of the optical feedback phenomenon in LDs is given by the rate equations first derived by Lang and Kobayashi [23]. This enables a behavioral model of an LD, which is subject to SM, to be built [24]. The emitted light is backscattered by the moving target, which modifies its frequency. The relation between the optical frequency of the emitted and backscattered waves is given by

$$x_0(t) - x_F(t) + C\sin[x_F(t) + \arctan(\alpha)] = 0 \qquad (1)$$

where $x_F(t)$ and $x_0(t)$ are the two phase signals with and without feedback, respectively, which are functions of the wavelengths with feedback $\lambda_F(t)$ and without feedback $\lambda_0(t)$, respectively, given by

$$x_F(t) = 2\pi \frac{D(t)}{\lambda_F(t)/2} = 2\pi\nu_F(t)\tau(t) \qquad (2)$$

$$x_0(t) = 2\pi \frac{D(t)}{\lambda_0(t)/2} = 2\pi\nu_0(t)\tau(t) \qquad (3)$$

where $\tau(t) = 2D(t)/c$ is the round trip time, c is the speed of light. $\nu_0(t)$ and $\nu_F(t)$ represent, respectively, the optical frequencies under free running conditions and with optical feedback. α is the linewidth enhancement factor, a physical characteristic of the laser. $\mathbf{C}$ is the feedback coupling factor, which depends on the reflection coefficient of the target and the distance to the target.

The expression of the OOP of an LD subject to feedback is given by

$$P_F(t) = P_0(1 + m\cos(x_F(t))) \qquad (4)$$

where P_0 is the emitted optical power in the free running state and m is the modulation index. After sampling and normalization of $P_F(t)$, the discrete-time-measured signal is given by $y(kT_e)$, where T_e is the sampling period, written as

$$y(kT_e) = y(k) = \cos[x_F(k)]. \qquad (5)$$

B. Model Behavior of the SM Signal

A lot of algorithms in signal processing require a model of the signal, which can be generated using schematic block diagrams. In our case, to represent the relation between the displacement $D(t)$ and the power $P(t)$ of the SM sensor, (4) and (7) have to be represented with elementary block diagrams, where (7) can be seen as an injective nonlinear relation $G[x_F(t); C, \alpha]$ between $x_F(t)$ and $x_0(t)$ given by

$$x_0(t) = x_F(t) + C\sin[x_F(t) + \arctan(\alpha)] \qquad (6)$$

$$= G[x_F(t); C, \alpha]. \qquad (7)$$

However, the required function is the relationship between $x_0(t)$ and $x_F(t)$, which can be defined as the "inverse" function of $G(.)$ given by

$$x_F(t) = F[x_0(t); C, \alpha]. \qquad (8)$$

The LD behavior depends significantly upon parameter C, whereas the OOP shape is only slightly affected by the value of parameter α [24], hence, α is not a relevant parameter. Here, we consider only the weak feedback, i.e., $C < 1$, $F(.)$ is easy to calculate numerically even if the inversion of the function $G(.)$ cannot be carried out analytically. An important property must be considered: if $x_0(t) = k\pi - \arctan(\alpha)$ for any integer k, then

$$x_F(t) = x_0(t) = k\pi - \arctan(\alpha) \qquad (9)$$

is a solution to (7).

A theoretical plot in Fig. 1 shows that the function $F(.)$ consists of the juxtaposition of small segments of curves $\mathbf{C}(k - 2), \mathbf{C}(k), \mathbf{C}(k + 2), \ldots$, with k being even. Each $\mathbf{C}(k)$ can be obtained from a translated nonlinear graph for a function $y = f(x; C)$, which is defined for $x \in [\pi, -\pi]$. Equation (10) shows that the calculation of a set of samples x_s from a set of linearly equally spaced points y_s between $-\pi$ and π is relatively simple. Then, y_s can be plotted as a function of x_s. The calculation of
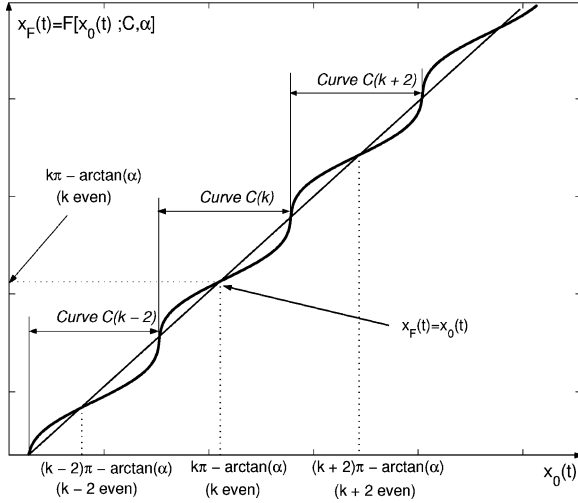
$$x = y + C\sin(y) \qquad (10)$$

Fig. 1. Plot of $x_F(t) = F[x_0(t); C; k]$ with $C < 1$. This graph consists of a juxtaposition of curves $\mathbf{C}(k-2)$, $\mathbf{C}(k)$, $\mathbf{C}(k+2)$, for even k.

with $x = x_0(t) + \arctan(\alpha)$ and $y(t) = x_F(t) + \arctan(\alpha)$ gives a set of point y_s between $[-\pi, \pi]$ for a set of samples x_s. The direct calculation of $y = f(x; C)$ has been carried out through a linear interpolation of data set x_s, y_s for a given x, which is expressed as

$$y = f(x; C) \approx f_{\text{INTERP}}(x; x_s, y_s, C). \tag{11}$$

This interpolation procedure has been achieved with a simple lookup table [24].

Moreover, the even integer number k with 2π intervals between 0 and $x_0(t)$ has to be determined. This number satisfies the inequality

$$(k-1)\pi - \arctan(\alpha) \leq x_0(t) \leq (k+1)\pi - \arctan(\alpha) \tag{12}$$

where $k \in \mathbb{N}$ is even. The solution to (12) is given by

$$k \text{ (even)} = 2 \operatorname{round}\left(\frac{x_0(t) + \arctan(\alpha)}{2\pi}\right) \tag{13}$$

where round is the rounding function toward the nearest integer. The interpolation procedure described in (11) and the calculation of k given in (13) can be represented with a simple and exact functional block diagram shown in Fig. 2 [24].

C. Extended Kalman Filter

The Kalman filter is a traditional efficient recursive filter that estimates the state of a dynamic system (here, the displacement of the target) from a series of incomplete and noisy measurements (like the OOP) [25]. For this purpose, a state model (or signal model) and an observation model are required. The displacement of the moving target is sinusoidal with a known frequency. This will be used in Section IV in order to find the FRF of the material.

For the signal model, we assume that the displacement increases and decreases quite gently, as in a mechanical vibration. The state vector $X(k)$ is composed of three elements: the displacement $x_1(k)$, the velocity $x_2(k)$ and $x_3(k)$, which is the unknown constant position within an error of $2\pi\lambda/2$. $x_3(k)$ is

a slowly varying process, which models the initial position as $x_3(k+1) = x_3(k) + w_3(k)$. $w_3(k)$ is a white gaussian noise. Amplitude fluctuations of $x_3(k)$ are controlled by the variance of w_3, $\sigma_{w_3}^2$. If $\sigma_{w_3}^2 = 0$, $x_3(k+1) = x_3(k)$, and the position is constant, whereas if $\sigma_{w_3}^2 > 0$, $x_3(k)$ is then a random walk, the amplitude of which increases with $w_3(k)$. The state model can then be written as

$$X(k+1) = AX(k) + W(k) \tag{14}$$

with the state vector $X(k) = [x_1(k), x_2(k), x_3(k)]^T$ where T is the transposition of the vector, and

$$A = \begin{bmatrix} \cos(2\pi f_0) & -\sin(2\pi f_0) & 0 \\ \sin(2\pi f_0) & \cos(2\pi f_0) & 1 \\ 0 & 0 & 1 \end{bmatrix} \tag{15}$$

is the state transition matrix and $W(k) = [0 \ 0 \ w_3(k)]^T$ is the state noise, which is white and zero-mean statistically independent, with variance $\sigma_{w_3}^2$. f_0 is the normalized frequency defined as the ratio of the frequency applied to the moving target and the sampling frequency.

The state vector is linked to the observation, i.e., the experimental data as

$$Y(k) = H[k, X(k)] + V(k) \tag{16}$$

where H is the theoretical relation between $Y(k)$ and $X(k)$, and $V(k)$ is the measurement noise, which is white and zero-mean statistically independent, with variance σ_v^2. The principle of the extended Kalman filter is based on the observation equation linearization around the current prediction of the state vector. If H is a linear relation, the traditional optimal Kalman filter is used instead. If H is nonlinear, the Kalman filter still can be used with a linearization of H between the state and the observation.

Using (5) and (8), the relation (16) can be rewritten as

$$Y(k) = \cos[F[x_1(k); C; \alpha] + V(k). \tag{17}$$

The observation $Y(k)$ is the normalized experimental OOP. In order to use an extended Kalman filter, this equation is linearized using a first-order Taylor development around $X(k)$ given by

$$C_0(k+1) = \frac{\partial H[k+1, X(k)]}{\partial X(k)}\Big|_{X(k) = \hat{X}(k+1|k)} \tag{18}$$

$$C_0(k+1) = [-\sin[F(x_1(k+1))]\frac{\partial F}{\partial k}(x_1(k+1)) \ 0 \ 0] \tag{19}$$

where $\frac{\partial F}{\partial k}(x_1(k+1))$ can be obtained from the numerical derivative of functional operator $F[x_0(t); C; \alpha]$. Using this linearization approach, the extended Kalman filter is suboptimal.

Based on the state model (14) and (16), we can then recursively calculate the estimation of the current state vector $\hat{X}(k|k)$, which is the output of the algorithm, and its estimation error covariance $P(k|k)$, via the Kalman filter recursions: $k = 1, 2, 3, \ldots$ [26].

For each k, $\hat{X}(k+1|k)$ is the state vector at $k+1$, knowing the other data at k. $P(k+1|k)$ is the covariance matrix of the state prediction error, i.e., the estimated error between the experimental value of $Y(k)$ at k and its prediction by the
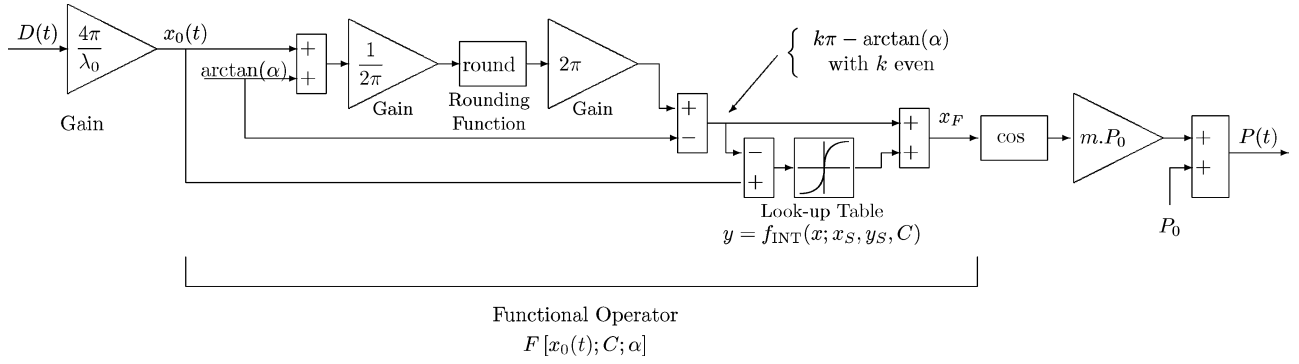
Fig. 2. Block diagram representation of signal transformations in an LD SM sensor. Behavioral representation of the functional operator $F[x_0(t); C; \alpha]$ for the SM LD sensor in the case of $C < 1$. The lookup table uses a set of samples $\{x_s, y_s\}$ to interpolate function $y = f(x; C)$. It gives the calculation of the OOP for a given displacement $D(t)$.

algorithm at $k - 1$. $Y(k|k-1) = C_0(k)\hat{X}(k|k-1)$ has to be determined in order to minimize this error. However, the data at $k = -1$, $k = -2$ are unknown. $\hat{X}(0|-1) = X_0$, the initial value of the state vector is roughly estimated from realistic experimental conditions. $P(0|-1) = P_0$, the confidence of this initial estimation, is evaluated according to how X_0 can be far from the real value (the higher the value of P_0, the less reliable the value of X_0).

The Kalman gain $L(k)$ at k is calculated first, using $P(k|k-1)$, which is the prediction of the estimation error covariance calculated at $k - 1$ as

$$L(k) = P(k|k-1)C_0^T(k)[C_0(k)P(k|k-1)$$
$$C_0^T(k) + R_V(k,k)]^{-1}.$$

The current state vector $\hat{X}(k|k)$, (i.e., the output of the algorithm) is next calculated as the roughly predicted state vector at $k - 1$, $\hat{X}(k|k-1)$, corrected by a term using the Kalman gain $L(k)$:

$$\hat{X}(k|k) = \hat{X}(k|k-1) + L(k)[Y(k) - C_0(k)\hat{X}(k|k-1)].$$

The current estimation error covariance is then computed as its predicted value at $k - 1$ also corrected by a term using the Kalman gain $L(k)$:

$$P(k|k) = P(k|k-1) - L(k)C_0(k)P(k|k-1). \qquad (22)$$

Estimated predictions of X and P at $k + 1$ are given by

$$\hat{X}(k+1|k) = A(k)\hat{X}(k|k) \qquad (23)$$

and

$$P(k+1|k) = A(k)P(k|k)A^T(k) + R_W(k,k) \qquad (24)$$

where $R_V(k,k)$ and $R_W(k,k)$ are the autocorrelation matrices of the process noise and the measurement noise, respectively.

III. SIMULATIONS

The extended Kalman filter algorithm has been tested with a simulated optical power. For a given simulated sinusoidal displacement [Fig. 3(a)] the corresponding optical output power is calculated [Fig. 3(b)], according to the method explained previously in Fig. 2.
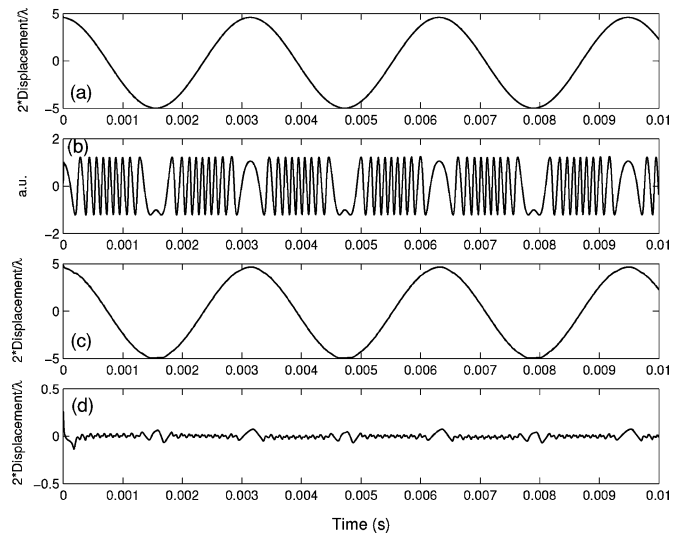

Fig. 3. (a) Simulated displacement of the target. (b) Simulated optical power of an LD focused on this moving target. (c) Reconstruction of the displacement using the extended Kalman filter. (d) Theoretical error, i.e., difference between (a) and (c).

For this example, the frequency displacement is 300 Hz, and its amplitude is $10\lambda/2$ (i.e., 4 μm), the sampling frequency is 240 kHz. The OOP is simulated with the values $C = 0.4$ and $\alpha = 4$.

The error of our algorithm is calculated as the difference between the simulated and the reconstructed displacement [Fig. 3(d)]. After a short time, the error is around $0.06\lambda/2$, i.e., around 30 nm for the semiconductor laser we use ($\lambda = 785$ nm).

IV. ANALYSIS FOR SURFACE DAMPING TREATMENT

A. Introduction

A damping layer is often used to solve a variety of resonant noise and vibrations problems, especially those associated with sheet metal structure vibrations. Such treatments can easily be applied to existing structures, and provide high damping capability over wide temperature and frequency ranges. These coating layer treatments are usually classified into two categories
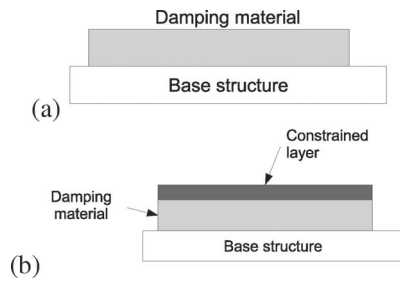
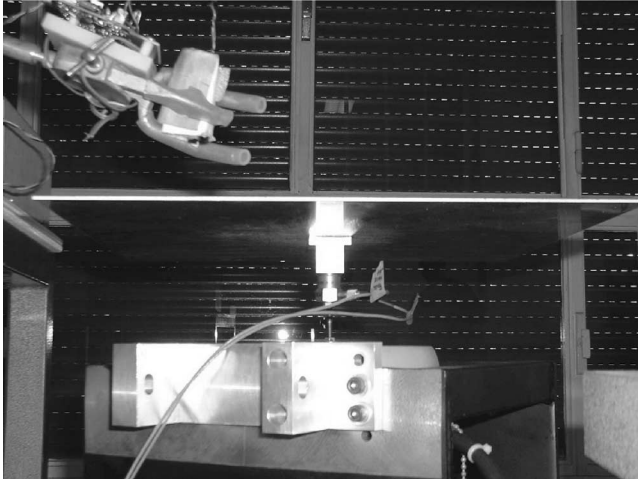Fig. 4. (a) Free-layer damping. (b) Constrained-layer damping.

Fig. 5. Photograph of the experimental setup: the shaker excites the plate, a PZT accelerometer measures the input acceleration, and the SM sensor measures the vibrations amplitude.
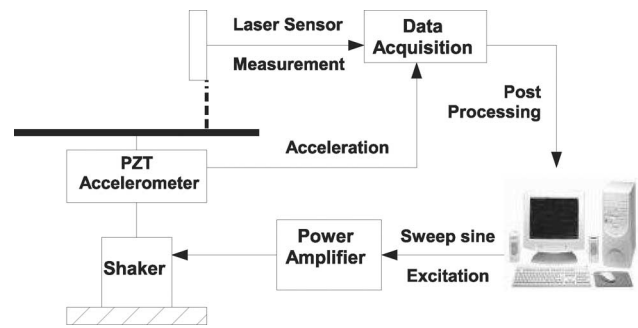

Fig. 6. Block diagram of the setup. Computer drives the shaker with a sweep sinusoidal signal, and records the data from the PZT acceleration sensor and the SM sensor or the commercial vibrometer. The proposed data are then postprocessed to plot the FRF.

according to whether the damping material is subject to extensional or shear deformation.

Fig. 4(a) shows a section of the target structure with a free layer damping (i.e., extensional damping). The damping material is sprayed on the structure or bonded using a pressure-sensitive core. The treatment can be coated on one or both sides of the structure.

When the base structure is deflected in bending, the viscoelastic damping material deforms primarily in extension and compression in planes parallel to the base structure. The hysteresis loop of the cyclic stress and strain thus, dissipates energy, while the degree of damping is limited by thickness and weight restrictions.

Fig. 4(b) shows the arrangement of a constrained-layer damping treatment (i.e., shear damping treatment). This consists of a sandwich of two outer elastic layers with a viscoelastic material as the core. When the base structure undergoes bending vibration, the viscoelastic material is forced to deform in shear because of the stiff upper layer. Constrained-layer damping is more efficient than the free-layer damping as more energy is dissipated and converted into heat during the work done by the shearing mode within the viscoelastic adhesive.

A typical constrained layer arrangement consists of a thin metal foil covered with a viscoelastic adhesive that can be used on an existing structure. The major difference between free and constrained layers is the influence of the thickness of the coating. For a constrained layer, the structural damping increases with the thickness till a maximum value, and remains constant when the thickness is more important while it still linearly increases with the thickness for a free layer.

The FRF is a method that allows the measurement of the efficiency of the surface damping treatment. It is calculated as the ratio of the displacement of the structure (i.e., the output displacement) to the input displacement at which the structure is subjected, on a logarithmic scale. This function enables us to know the performance of the structure at resonance, and to measure the structural damping [27]–[29].

The damping is determined through the comparison of the average vibration level (AVL); the higher the level, the weaker is the damping (see the Appendix).

B. Experimental Setup

The schematic of the measurement system for FRF is illustrated in Fig. 6. A shaker, which is driven by a sweeping sinusoidal signal using a Labview program, excites the plate under test (Fig. 5). The dimensions of the plates used are 350 mm $\times$ 350 mm $\times$ 2 mm, and the boundary conditions are free–free. A piezoelectric transducer (PZT) sensor positioned between the shaker and the plate measures the acceleration. Our SM sensor using an LD with a 785-nm wavelength then measures the response displacement. A commercial calibrated vibrometer (Polytec CLV-700) was used as the reference sensor.

Two signals from the PZT sensor and the SM sensor (or the commercial vibrometer) were digitized by a data acquisition card. After postprocessing of the SM signal with the proposed extended Kalman filter algorithm written using Matlab, the displacement of the plate was obtained. Numerical integration of the signal of the vibrometer results in a reference measurement of the target displacement. The ratio of the displacement of the structure (i.e., the output displacement) to the input displacement (given by a double integration of the PZT accelerometer) is then calculated for each excitation frequency.

The joint between the shaker and the plate is realized with a piece having a T-form, which is bonded onto the plate. Hence, excitation of the shaker can be applied on every part of the plate.
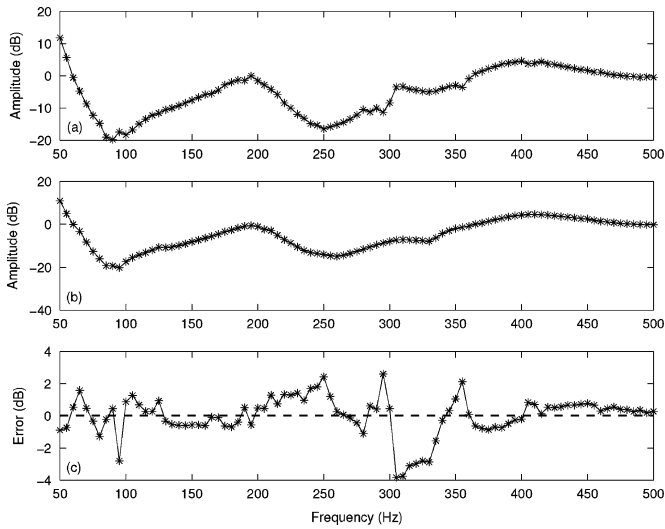
Fig. 7. FRF of an EAR plate subject to sinusoidal excitation (a) from SM sensor, (b) from commercial vibrometer, and (c) error calculated as the difference between (a) and (b).
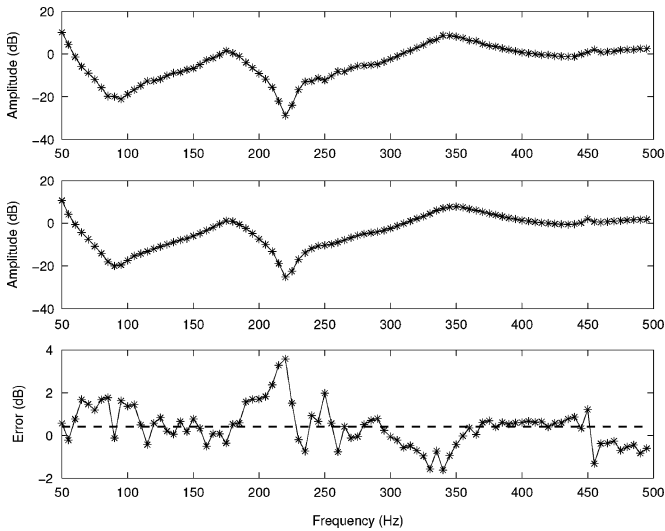

Fig. 8. FRF of a SMAC plate submitted to sinusoidal excitation (a) from SM sensor, (b) from commercial vibrometer, and (c) error calculated as the difference between (a) and (b).

We chose to apply the excitation at the center of an aluminum plate (base structure-AU4G) with a thickness of 2 mm.

C. Results and Discussion

Fig. 7 represents the FRF measurement for the aluminium plate studied with a free layer [an EAR (composite material) plate of thickness 5 mm], using first the SM sensor [Fig. 7(a)] and the commercial vibrometer [Fig. 7(b)]. The same experiment has been achieved with a constrained layer [a SMAC® (composite material) plate thickness of 4 mm] (Fig. 8). In both cases, the maximum error is approximately ±4 dB. There is a good agreement between both methods.

Fig. 9 shows the experimental results for the 2 mm-excited aluminium plate. The damping is very small due to shape peaks. Figs. 7 and 8 when compared to Fig. 9 show the effect of the
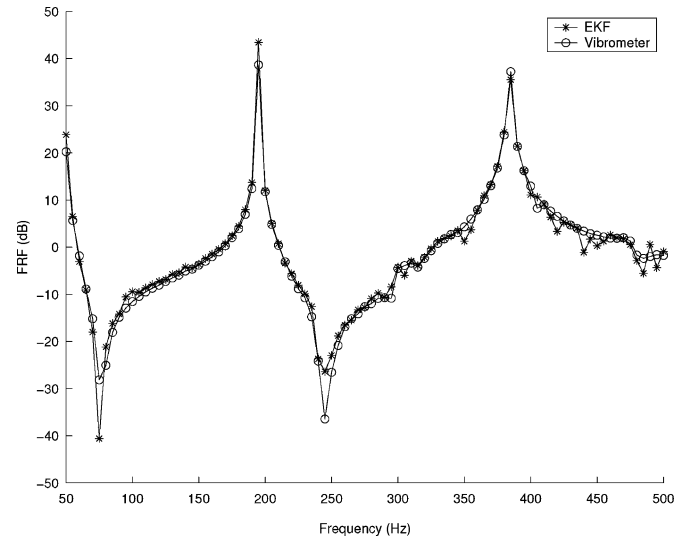

Fig. 9. FRF of a plate without surface damping treatment from the SM sensor using the extended Kalman filter and from the vibrometer.

added layer on the vibration. The FRF is decreased to 20 dB, and a damping is present.

These results show that the EAR plate seems to have the best performance, i.e., the lower vibration amplitudes. This can be explained by the thicknesses and the densities of both plates being different. Both coating permit an important damping of the structure. The amplitude of the output displacement is strongly decreased, reducing at the same time, the problem of noise transmission to other structures.

The frequency limit of this SM sensor cannot be determined easily because it depends on the mechanical displacement frequency and the amplitude of this displacement. Indeed, the number of OOP fringes generated is proportional to the amplitude of this displacement. The larger the amplitude, the higher the sampling frequency of the OOP will have to be increased, in order to sample every fringe.

V. CONCLUSION

An SM displacement sensor with the LD under weak feedback was designed in order to achieve accurate vibration displacement measurements. For this purpose, an extended Kalman filter was computed by using a behavioral model of the SM signal. This simple sensor was tested on plates in order to measure the FRF when coated and uncoated with a passive damping layer. Experimental results were successfully compared to those obtained with a calibrated commercial vibrometer, which is far more costly. Due to its relatively low cost, our sensor can be duplicated in order to achieve several data acquisitions on the considered plate for each frequency simultaneously.

In this paper, we measured the FRF at one point in order to demonstrate the efficiency of a damping treatment. However, 10 points of measurements are required to determine the performance characteristics of a plate (see Appendix). A network of SM sensors can, thus, allow the AVL to be measured rapidly, in order to determine the global performance of the plate. Such
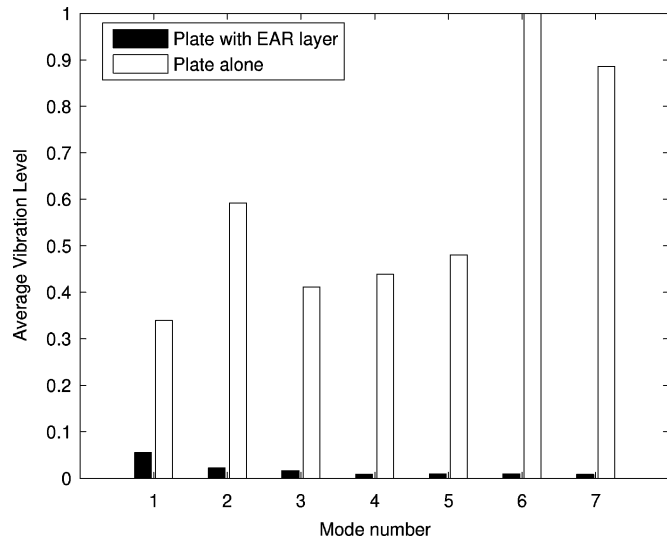
Fig. 10.   Results for a plate with a layer of EAR coating.

a network can use, for example, ten sensors simultaneously, since a single sensor coupled with a scanning XY mirror is more costly and less robust mechanically. This SM sensor network can be cost effective and of great interest to achieve online modal analysis of mechanical pieces.

APPENDIX

AVL

The AVL is a global parameter required to determine the behavior of a mechanical piece subject to vibration. AVL takes into account the acceleration for an eigenvalue, i.e., corresponding to a peak on the FRF, which can be given by

$$\text{AVL}_j = \frac{1}{n} \sqrt{\sum_{i=1}^{n} \gamma_i^2}$$

where n is the number of measured points, and γ_i is the acceleration at the point i for eigenvalue j.

This parameter allow the performance of a structure to be quantified. In fact, if the measurements were realized at an insufficient number of points, the FRF can be truncated, as some points can be an antinode of a mode shape.

The lager the number of measured points, the more accurate the AVL value will be (i.e., closed to the theoretical value). However, to measure the performance of a plate, it has been proved experimentally that 10 points of measurement results in an AVL value with sufficient precision. As an example, Fig. 10 represents the respective responses of a plate without damping and with a layer of EAR for the first seven modes. For each frequency, ten measurements have been performed at different points of the plate, the laser sensor being translated manually between each FRF acquisition. By averaging the results obtained from a given sample of ten measurements, the eigen frequencies of the coated plate can be determined with a better accuracy.

REFERENCES

[1] M. D. Rao, "Recent applications of viscoelasic damping for noise control in automobiles and commercial airplanes," *J. Sound Vib.*, vol. 262, pp. 457–474, 2003.

[2] A. D. W. McKie, J. W. Wagner, J. B. Spicer, and J. B. D. Jr, "Dual-beam interferometer for the accurate determination of surface-wave velocity," *Appl. Opt.*, vol. 30, pp. 4034–4039, 1991.

[3] J. Huang and J. D. Achenbach, "Dual-probe laser interferometer," *J. Acoust. Soc. Am.*, vol. 90, pp. 1269–1274, 1991.

[4] S. Hurlebaus and L. Jacobs, "Dual-probe laser interferometer for structural health monitoring," *J. Acoust. Soc. Am.*, vol. 119, pp. 1923–1925, 2006.

[5] D. J. Mead, *Passive Vibration Control*, 2nd ed.   Paris, France: Librairie Polytechnique CH, 1961.

[6] T. Bosch, N. Servagent, and S. Donati, "Optical feedback interferometry for sensing application," *Opt. Eng.*, vol. 40, no. 1, pp. 1–7, 2001.

[7] W. M. Wang, K. T. V. Grattan, A. W. Palmer, and W. J. O. Boyle, "Self-mixing interference inside a single-mode diode laser for optical sensing applications," *IEEE J. Lightw. Technol.*, vol. 12, no. 9, pp. 1577–1587, Sep. 1994.

[8] P. de Groot, "Unusual technique for absolute distance measurement," *Opt. Eng.*, vol. 40, pp. 28–32, 2001.

[9] S. Merlo and S. Donati, "Reconstruction of displacement waveforms with a single-channel laser-diode feedback interferometer," *IEEE J. Quantum Electron.*, vol. 33, pp. 527–531, 1997.

[10] L. Scalize, Y. Yu, G. Guido, G. Plantier, and T. Bosch, "Self-mixing laser diode velocimetry: Application to vibration and velocity measurement," *IEEE Trans. Instrum. Meas.*, vol. 53, no. 1, pp. 223–232, Feb. 2004.

[11] S. Shinohara, A. Mochizuki, H. Yoshida, and M. Sumi, "Laser doppler velocimeter using the self-mixing effect of a semiconductor laser diode," *Appl. Opt.*, vol. 25, pp. 1417–1419, 1986.

[12] T. Bosch, N. Servagent, and M. Lescure, "A laser displacement sensor using the self-mixing effect for modal analysis and defect detection," *IEEE J. Instrum. Meas.*, vol. 46, no. 4, pp. 847–850, Aug. 1997.

[13] S. K. Ozdemir, S. Takamiya, S. Ito, S. Shinohara, and H. Yoshida, "Self-mixing laser speckle velocimeter for blood flow measurement," *IEEE Trans. Instrum. Meas.*, vol. 49, no. 5, pp. 1029–1035, Oct. 2000.

[14] S. Donati, *Electro-Optical Instrumentation: Sensing and Measuring with Lasers.*   Englewood Cliffs, NJ: Prentice-Hall, 2004.

[15] T. Bosch, C. Bes, L. Scalise, and G. Plantier, *Self-Mixing Sensors in Encyclopedia of Sensors*, C. A. Grimes, E. C. Dickey, and M. V. Pishko, Eds. Valencia, CA: American Scientific, 2006.

[16] N. Servagent, F. Gouaux, and T. Bosch, "Measurements of displacement using the self-mixing interference in a laser diode," *J. Opt.*, vol. 29, pp. 168–173, 1998.

[17] N. Servagent, T. Bosch, and M. Lescure, "Design of a phase-shifting optical feedback interferometer using an electro-optic modulator," *IEEE J. Sel. Topics Quantum Electron.*, vol. 6, no. 5, pp. 798–802, Sep./Oct. 2000.

[18] S. Donati, G. Giulani, and S. Merlo, "Laser diode feedback interferometer for measurement of displacements without ambiguity," *IEEE J. Quantum Electron.*, vol. 31, no. 1, pp. 113–119, Jan. 1995.

[19] G. Plantier, N. Servagent, T. Bosch, and A. Sourice, "Real-time tracking of time-varying velocity using a self-mixing laser diode," *IEEE Trans. Instrum. Meas.*, vol. 53, no. 1, pp. 109–115, Feb. 2004.

[20] G. Plantier, C. Bes, and T. Bosch, "Auto adaptive signal processing of a laser diode self-mixing displacement sensor," *Proc. 22nd IEEE Instrum. Meas. Conf.*, 2005, vol. 2, pp. 1013–1017.

[21] C. Bes, T. Bosch, G. Plantier, and F. Bony, "Characterization of a self-mixing displacement sensor under moderate feedback," *Opt. Eng.*, vol. 45, no. 8, pp. 084 402.1–084 402.6, Aug. 2006.

[22] K. Petermann, *Laser Diode Modulation and Noise.*   Norwell, MA: Kluwer, 1991.

[23] K. Kobayashi and R. Lang, "External optical feedback effects on semiconductor injection laser properties," *IEEE J. Quantum Electron.*, vol. 16, no. 3, pp. 347–355, Mar. 1980.

[24] G. Plantier, C. Bes, and T. Bosch, "Behavioral model of a self-mixing laser diode sensor," *IEEE J. Quantum Electron.*, vol. 41, no. 9, pp. 1157–1167, Sep. 2005.

[25] M. S. Grewal and A. P. Andrews, *Kalman Filtering: Theory and Practice.* Englewood Cliffs, NJ: Prentice-Hall, 1993.

[26] S. M. Kay, *Fundamentals of Statistical Signal Processing-Estimation theory.* Englewood Cliffs, NJ: Prentice-Hall, 1993.

[27] R. Caraciolo, A. Gasparetto, and M. Giovagnoni, "Measurement of the isotropic dynamic Young's modulus in a seismically excited canteliver beam using a laser sensor," *J. Sound Vib.*, vol. 231, pp. 1339–1353, 2000.

[28] R. Caraciolo, A. Gasparetto, and M. Giovagnoni, "Application of causality check and of the reduced variables method for experimental determination of young's modulus of a viscoelastic material," *Mech. Mater.*, vol. 33, pp. 693–703, 2001.

[29] R. Caraciolo, A. Gasparetto, and M. Giovagnoni, "An experimental technique for complete dynamic characterization of a viscoelastic material," *J. Sound Vib.*, vol. 272, pp. 1013–1032, 2001.

Caroline Bés was born in Pezenas, France, in 1979. She received the graduate degree in spatial telecommunications from the National Engineering School of Aeronautics and Space (SUPAERO), Toulouse, France, in 2003. She is currently working toward the Ph.D. degree in optoelectronic engineering at the École Nationale Supérieure d'Électrotechnique, d'Électronique, d'Informatique, d'Hydraulique et des Télécommunications, Toulouse, France.

Her current research interests include vibration and velocity measurements for industrial applications, data acquisition, and signal processing.

Victorien Belloeil was born in Saint Brieuc, France, in 1980. He received the graduate degree from the Ecole Supérieure d'Ingénieurs de Marseille (ESIM), Marseille, France, in 2003. He is currently working toward the Ph.D. degree in mechanical engineering at the École Nationale Supérieure de l'Aéronautique et de l'Espace (SUPAERO), Toulouse, France.

His current research interests include the diminution of noise in helicopter cabins with a new concept of passive vibration control. This research is realized with the Dynamics Departement of EUROCOPTER, and the Departement of Mechanical Engineering of the Ecole Nationale Supérieure d'Ingénieurs de Constructions Aéronautiques (ENSICA).

Guy Plantier (M'00) was born in Ales, France, in 1961. He received the title of Engineer from the National School of Engineers of Brest, France, in 1984, and the Ph.D. degree in acoustics from the University of Le Mans, France, in 1991.

He spent two years in the Acoustics and Vibrations Group, Sherbrooke University, Sherbrooke, QC, Canada. In 1993, he joined the Ecole Suprieure d'lectronique de l'Ouest (ESEO), Angers, France, where he is currently the Head of the Electronics and Physics Department. His current research interests include signal processing for instrumentation, vibration, and velocity measurements, laser Doppler anemometry, active noise control of sounds and vibrations, and communications.

Yves Gourinat received the Ph.D. degree in mechanics.

He is currently a Professor at the École Nationale Supérieure de l'Aéronautique (SUPARO) et de l'Espace, Toulouse, France, where he is also the Head of the Department of Mechanics, Structures and Materials. He is a Senior Advisor for the Délégation Générale pour l'Armement in the fields of aircraft architecture and missile structure. He is the author of the manual for dynamics of structure used in French aerospace engineering schools. His current research interests include damping and irreversibility in aerospace structures.

Prof. Gourinat was appointed Chairman of the Mechanical Session of the First France-China Aerospace Research Workshop, held in 2006.

Thierry Bosch (M'93) received the Ph.D. degree in optoelectronics from the Institut National des Sciences Appliques.

He is currently a Professor at the École Nationale Suprieure d'Électrotechnique, d'Électronique, d'Informatique, d'Hydraulique et des Télécommunications (ENSEEIHT), Toulouse, France, where he is also the Director of the Electronics Laboratory (LEN7). He was a Guest Co-Editor for the *Journal of Optics* (June 1998, November 2002) and *Optical Enginering* (January 2001) on Distance/Displacement Measurements by Laser Techniques. He was also a Co-Editor of the volume entitled *Selected Papers on Laser Distance Measurements* (Bellingham, WA: SPIE, 1995). His current research interests include laser industrial instrumentation development including range finding techniques, vibration and velocity measurements.

Dr. Bosch created the International Conference ODIMAP. He is currently Chairman of the IEEE Instrumentation and Measurement Society Technical Committee on "Laser and Optical Systems" and serves as an Associate Editor of the IEEE TRANSACTIONS ON INSTRUMENTATION AND MEASUREMENT since 1997.